SAND2017-3107C

Data-driven Adaptive Physics Modeling for Turbulence Simulations

J. Ling *
Sandia National Labs, Livermore, CA, 94550, USA
Andrew Kurzawski
†*University of Texas at Austin, Austin, TX, 78712, USA*

For many aerospace applications, there exists significant demand for more accurate turbulence models. Data-driven machine learning algorithms have the capability to accurately predict when Reynolds Averaged Navier Stokes (RANS) models will have increased model form uncertainty due to the breakdown of underlying model assumptions. These machine learning models can be used to adaptively trigger relevant model corrections in the regions they are needed. This paper presents a framework for data-driven adaptive physics modeling that leverages known RANS model corrections and proven machine learning methods. This adaptive physics modeling framework is evaluated for two case studies: fully developed turbulent square duct flow and flow over a wavy wall. It is demonstrated that implementing model corrections zonally based on machine learning classification of where underlying RANS model assumptions are violated can achieve the same accuracy as implementing those corrections globally.

Nomenclature

b_{ij}	Normalized Reynolds stress anisotropy tensor
f_{ML}	Zonal factor
k	Turbulent kinetic energy
R_{ij}	Mean rotation rate tensor
S_{ij}	Mean strain rate tensor
Sc_t	Turbulent Schmidt number
$\overline{u_i' u_j'}$	Reynolds stress component
II_b	Second invariant of the Reynolds stress anisotropy tensor
ϵ	Turbulent dissipation rate
Θ	Scalar concentration
ν_t	Eddy viscosity

I. Introduction

Reynolds Averaged Navier Stokes (RANS) turbulence models are widely used in aerospace applications because the high Reynolds numbers of aerodynamic flows preclude the use of wall-resolved Large Eddy Simulation (LES) or Direct Numerical Simulation (DNS) as part of the design process. However, the reliance of RANS simulations on empirical closures to model turbulent transport makes them susceptible to increased uncertainty. When the model closures make erroneous assumptions or do not fully model the physics of the flow, the simulation results are prone to model form error. Because of this model form error, RANS simulations often give poor performance in many flows of engineering relevance.[1–4]

*Harry S. Truman Fellow, Thermal/Fluids Science and Engineering Department
†PhD Candidate, Mechanical Engineering Department

RANS model form uncertainty arises when one of the underlying model assumptions is violated. For example, if the Reynolds stress tensor is significantly anisotropic, then a linear eddy viscosity model that dictates a direct proportionality between the Reynolds stresses and the mean strain rate may be inadequate. If the turbulent transport of momentum is counter to the velocity gradient, then a negative eddy viscosity is required to provide the correct Reynolds stress value. In these flows, the common assumption of a non-negative eddy viscosity would be violated. Thus, RANS model form uncertainty may arise from different sources depending on the physics of the flow. In flows where the anisotropy or counter-gradient transport affects the mean flow field, this model form uncertainty will cause inaccuracy in the predictions of the quantities of interest.

Various corrections and variations of RANS have been proposed to mitigate these sources of uncertainty. Algebraic Stress Models (ASM) and nonlinear eddy viscosity models have been proposed to provide improved Reynolds stress anisotropy predictions.[5–8] Reynolds Stress Transport Models (RSTM) solve a separate equation for each component of the Reynolds stresses, and therefore do not rely on a scalar eddy viscosity. If these models are still inadequate, high fidelity simulations such as Large Eddy Simulations (LES) or Direct Numerical Simulations (DNS) can provide improved predictions at the cost of increased computational requirements.

While ASM and non-linear eddy viscosity models can enable improved RANS predictions without the drastic increase in computational cost imposed by LES, they are not always easy to use in practice. Gatski and Speziale[6] remarked that in flows with high mean strain rates, some algebraic stress models fail to converge. Belhoucine et al.[9] also reported that algebraic stress models can cause poor stability and slow convergence in complex flows. These same complaints have surfaced in several other studies.[10–13] To gain convergence with these anisotropic models, several strategies can be employed: the flow can be initialized with the solution from a linear eddy viscosity model; the iterations can be under-relaxed; a mesh of higher quality can be used; the higher order model can be blended with the linear eddy viscosity model to produce a hybrid formulation. Often, multiple of these strategies are employed to achieve convergence. However, because of the added difficulty often associated with implementing these anisotropic models, combined with the fact that it is usually unclear whether they will yield improved results, they are not widely used–simple linear eddy viscosity models remain the most popular among RANS models.

Recently, Gorle et al.[4] presented a marker that can flag regions of high RANS uncertainty based on when the flow field deviates from parallel shear flow, the flow regime for which most RANS models were calibrated. Ling and Templeton[14] built on this concept by developing machine learning classifiers which can predict in which regions of a flow specific underlying RANS model assumptions are violated, based on the local RANS flow variables. Whereas the marker of Gorle et al. was based on domain knowledge and physical intuition alone, the classifiers of Ling and Templeton leveraged high-dimensional data-driven algorithms and were trained on a database of flow configurations for which high fidelity simulation data were available. These machine learning classifiers achieved significantly reduced classification error rates ($\sim 3\times$ lower across the database of validation cases) relative to the physics-based classifier of Gorle et al. in determining regions of high Reynolds stress anisotropy. These classifiers provide the opportunity to implement adaptive physics modeling (APM), in which corrections are applied only in the regions where they are needed. Based on which underlying model assumption is violated in a given region of the flow, the appropriate model correction can be applied. This kind of adaptive physics modeling has not previously been explored.

Adaptive modeling for turbulence simulations most often refers to adaptive mesh refinement, in which the mesh is locally refined during the simulation as needed to satisfy accuracy requirements.[15] Richardson extrapolation can be used to determine where local refinement is necessary to reduce numerical discretization errors. Adaptive mesh refinement can provide improved predictive accuracy in unsteady flows for which isotropic grid refinement would be computationally infeasible.[16] However, in many cases, RANS uncertainty is not driven by discretization error, but by model form error. In these cases, adaptive mesh refinement will not yield significant improvements in accuracy–improved model forms are required.

The objective of the present study is to present a framework for data-driven adaptive physics modeling, in which machine learning classifiers are used to adaptively trigger RANS model corrections in the regions they are needed. The key question investigated here is whether implementing RANS model corrections only in the regions indicated by machine learning classification can recover the same accuracy as implementing the RANS model corrections globally. The APM framework is quite general, and could be applied to mitigate many sources of model form uncertainty using either previously published higher order RANS models or new data-driven models such as those suggested by Zhang et al.[17] and Ling et al.[18] This paper will investigate the

APM framework in the context of two RANS model corrections: one for the Reynolds stresses, and another for the turbulent scalar fluxes. Section II will discuss the specific model corrections used and how the machine learning methods were used to trigger them zonally. Section III will present results from the adaptive physics modeling strategy for two flows: turbulent duct flow and flow over a wavy wall. Both simulation accuracy and convergence properties will be discussed. Finally, Section IV will present conclusions and promising next steps for this research.

II. Implementation of Adaptive Modeling Framework

Adaptive physical modeling is a general framework in which model corrections are applied in regions flagged by machine learning classifiers. These corrections could consist of higher order RANS models, Reynolds Stress Transport Models, or LES. In the present study, anisotropic RANS models are considered as potential corrections for regions where using a simple isotropic linear eddy viscosity model would be insufficient.

A. Eddy Viscosity Models

Most two-equation RANS models rely on an eddy viscosity model for the Reynolds stresses. The most widespread model is the Linear Eddy Viscosity Model (LEVM), also known as the Boussinesq model:

$$\overline{u_i' u_j'} = \frac{2}{3} k \delta_{ij} - 2\nu_t S_{ij} \tag{1}$$

In Eq. 1, $\overline{u_i' u_j'}$ is the Reynolds stress tensor, k is the turbulent kinetic energy, ν_t is the eddy viscosity, and $S_{ij} = \frac{1}{2}(\frac{dU_i}{dx_j} + \frac{dU_j}{dx_i})$ is the mean strain rate tensor. Not only is this model simple and easy to implement, but it also has the convenient property of aiding convergence by adding extra diffusion into the momentum equations. However, this model is known to give poor predictions in many flows of engineering interest, including flows with curvature, separation, and impingement.[8,13]

To remedy these shortcomings of the LEVM, several non-linear eddy viscosity models have been proposed.[5,8,19] These non-linear models represent the Reynolds stress tensor in terms of quadratic, cubic, quartic, and fifth-order products of the mean strain rate tensor S_{ij} and mean rotation rate tensor R_{ij}. Pope[19] demonstrated that a fifth-order eddy viscosity model was the most general possible representation of an eddy viscosity model depending on only S_{ij} and R_{ij}–higher order polynomial representations can be reduced to fifth-order products using the Caley Hamilton theorem. These non-linear models have more flexibility to properly represent the Reynolds stress anisotropy. However, they have not gained widespread usage because they often have degraded stability properties relative to the LEVM. Non-linear models result in tighter coupling between the velocity components, since the divergence of the Reynolds stresses will involve the derivatives of all components of the velocity vector. Furthermore, in regions of large velocity gradients, the high order products of S_{ij} and R_{ij} can result in numerical instability.

In the present study, a Quadratic Eddy Viscosity Model (QEVM) is compared to the LEVM. The QEVM is based loosely on Craft's cubic eddy viscosity model,[8] but excludes the cubic terms which are often responsible for increased instability. The QEVM representation of the Reynolds stress tensor is given by:

$$\begin{aligned} \overline{u_i' u_j'} = \; & \frac{2}{3} k \delta_{ij} - 2\nu_t S_{ij} + C_1 \frac{\nu_t k}{\tilde{\epsilon}} (4 S_{ik} S_{kj} - \frac{4}{3} S_{kl} S_{kl} \delta_{ij}) \\ & + C_2 \frac{\nu_t k}{\tilde{\epsilon}} (4 R_{ik} S_{kj} + 4 R_{jk} S_{ki}) + C_3 \frac{\nu_t k}{\tilde{\epsilon}} (4 R_{ik} R_{jk} - \frac{4}{3} R_{kl} R_{kl} \delta_{ij}) \end{aligned} \tag{2}$$

In Eq. 2, $\tilde{\epsilon}$ is the isotropic dissipation,[8,20] and C_1, C_2, and C_3 are model coefficients set to -0.1, 0.1, and 0.26 respectively. While this model does not have the versatility of a full fifth-order eddy viscosity model, it can more fully represent the Reynolds stress anisotropy than the LEVM while retaining enough numerical stability to be applied in complex flows.

B. Turbulent Scalar Flux Models

In order to solve for a scalar concentration Θ, a closure model is needed for the turbulent scalar fluxes, $\overline{u_i' \Theta'}$, which represent the transport of the scalar due to turbulent fluctuations. The most widespread model for the

turbulent scalar fluxes is the Gradient Diffusion Hypothesis (GDH) with a fixed turbulent Schmidt number Sc_t:

$$\overline{u_i'\Theta'} = -\frac{\nu_t}{Sc_t}\frac{d\Theta}{dx_i} \tag{3}$$

The GDH model is simple, and like the LEVM, tends to improve stability by adding extra diffusion into the system of equations. Also like the LEVM, it does not predict the turbulent scalar flux anisotropy adequately in many flows of interest.

Daly and Harlow[21] proposed the Generalized Gradient Diffusion Hypothesis (GGDH) to provide more accurate turbulent scalar flux anisotropy predictions:

$$\overline{u_i'\Theta'} = -C_\theta \frac{k}{\epsilon}\overline{u_i'u_j'}\frac{d\Theta}{dx_j} \tag{4}$$

In the GGDH model, the tunable parameter C_θ is usually set to a value of 0.3. In this study, a hybrid GGDH formulation was employed, using a linear blend between GDH and GGDH to improve stability.

The main advantages of the LEVM and GDH models are their simplicity and good convergence properties. This simplicity comes at the cost of reduced ability to capture flow anisotropy. The QEVM and GGDH models, while less numerically stable, can provide improved anisotropy predictions.

C. Machine Learning Classifiers

Because the QEVM and GGDH can negatively impact the simulation convergence and stability, it would be desirable to only use these models when they are required. If the Reynolds stresses and turbulent scalar fluxes are not significantly anisotropic, then the QEVM and GGDH would most likely not improve the velocity field or concentration distribution predictions, but could still result in numerical instabilities. In order to use the higher order models only when they are needed, a technique for determining when the flow is anisotropic is required.

Ling and Templeton[14] used machine learning techniques to develop a classifier that flags regions of high Reynolds stress anisotropy. Machine learning comprises a set of data-driven algorithms that can be used for regression, classification, and clustering. Machine learning includes simple algorithms like linear regression, as well as more complex algorithms such as neural networks, random forests, and support vector machines. The common thread among these algorithms is that they are data-driven–they build a model based on the available data. These methods can process big, high-dimensional data sets, such as those generated in computational fluid dynamics, to discern underlying patterns and structure in the data. Ling and Templeton cross-validated their classifiers across a broad range of flows, including jets in crossflow, a cube in crossflow, channel flow, duct flow, and flow over a wavy wall. The classifier for regions of high Reynolds stress anisotropy was shown to have good accuracy (89%) across this cross-validation database. The machine learning classifier used local RANS flow variables, including the mean velocity gradient, the pressure gradient, and the turbulent kinetic energy, to make binary predictions about whether or not the flow was significantly anisotropic. The classifier was trained using high fidelity DNS and LES data, from which the true Reynolds stress anisotropy could be extracted. The anisotropy of the flow was quantified using the Reynolds stress anisotropy tensor invariants. For the non-dimensional Reynolds stress anisotropy tensor $b_{ij} = \frac{\overline{u_i'u_j'}}{2k} - \frac{1}{3}\delta_{ij}$, the second invariant $II_b = b_{ij}b_{ji}$ will vary from 0 in isotropic turbulence to 0.67 in one-component turbulence.[22,23] A threshold value of 0.167, corresponding to two-component turbulence, was used to designate flow that was significantly anisotropic. The machine learning classifier was trained to flag regions of the flow in which $II_b > 0.167$; this flag can be used to activate the zonal model corrections in those regions.

D. Zonal Implementation of RANS Model Correction

Because the machine learning model classifies each point in the flow as having either isotropic or anisotropic Reynolds stresses, for any given flow it can isolate the specific regions in which a non-linear eddy viscosity model should be applied. This approach, in which the machine learning classifier is used to determine in which regions of the flow a correction term should be applied, has been termed the "zonal" approach. Therefore, a zonal QEVM implementation would use the default LEVM in regions of the flow indicated to be isotropic by

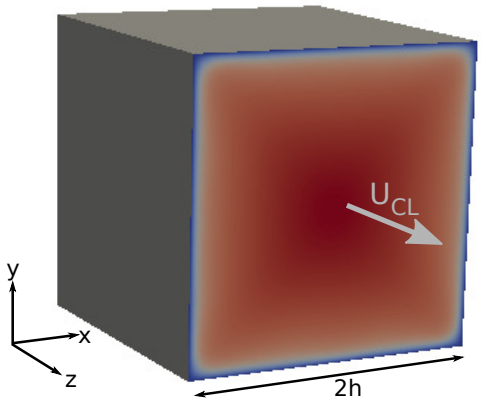

Figure 1. Schematic of duct flow configuration with coordinate axes.

the machine learning classifier, but would use the QEVM in anisotropic regions. For cases involving scalar transport, this same machine learning classifier can be used to trigger the use of the GGDH. Because scalar flux anisotropy is often caused by the same underlying flow features as Reynolds stress anisotropy (e.g. the no-penetration condition near a wall or coherent vortices), the same machine learning classifier was used to trigger the GGDH as the QEVM. Therefore, in the zonal approach, the GGDH is applied in the same regions as the QEVM.

The machine learning classifiers were used to provide a zonal factor f_{ML} that activated the higher order models. For example, in the case of zonal QEVM, the Reynolds stresses were calculated as:

$$(\overline{u_i' u_j'})_{\mathrm{ZONAL}} = (1 - f_{\mathrm{ML}})(\overline{u_i' u_j'})_{\mathrm{LEVM}} + f_{\mathrm{ML}}(\overline{u_i' u_j'})_{\mathrm{QEVM}} \tag{5}$$

While the machine learning classifiers predict a strictly binary f_{ML}, a Gaussian filter was used to smooth the boundaries of the zonal regions, such that the higher order models were blended in linearly at these boundaries as dictated by Eq. 5, providing a smooth transition between models.

In the present study, the zonal method was implemented in a two-step process: the default LEVM simulation was run to convergence, and the machine learning classifiers described in Section C were then applied to the LEVM results to determine in which regions the anisotropic models should be applied. This mask was then read into the flow solver, which then solved the flow again, this time using the anisotropic models in the indicated regions. In the future, this two-step process will be combined such that the machine learning classifiers are queried during runtime and the appropriate correction terms are activated as needed.

III. Case Studies

The APM framework for zonal corrections is investigated here for two flow cases: fully developed turbulent duct flow and flow over a wavy wall with scalar injection. These two flow cases were chosen because in each of them, anisotropy is known to significantly affect the mean field variables. In the duct flow case, results will be compared using the LEVM, QEVM, and zonal QEVM. For the wavy wall flow case, a scalar transport equation is also solved, so results will be compared using LEVM with GDH, QEVM with GGDH, and zonal QEVM with GGDH. In both cases, DNS data are available to compare against.

A. Fully Developed Turbulent Duct Flow

1. Simulation Set-Up

The flow configuration, shown schematically in Fig. 1, was that of fully developed turbulent square duct flow of Reynolds number 3500 based on the bulk velocity and duct half-height h. This is an interesting configuration to investigate because of the important role that Reynolds stress anisotropy plays in this flow. It is one of the simplest flows to present secondary flows of the second kind, which are stress-induced

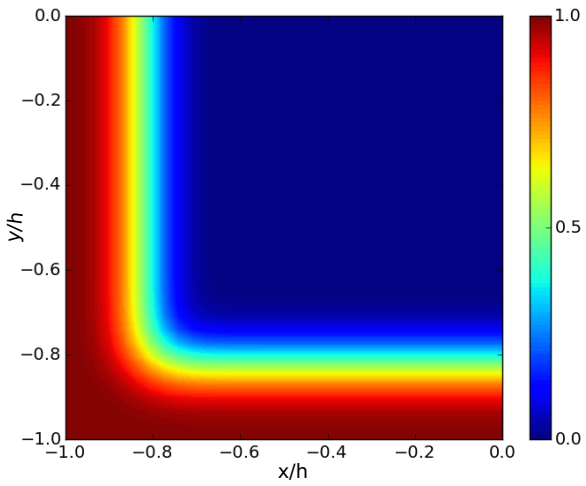

Figure 2. Mask of f_{ML} used for zonal implementation of QEVM. Because of the symmetry properties of this flow, only one quarter of the duct was modeled in RANS.

secondary flows .[24] These secondary flows consist of paired corner vortices in each quadrant of the duct, which are not predicted by linear eddy viscosity models. A previous study by Gnanga et al.[25] reported that a non-linear eddy viscosity model was able to predict corner vortices in their fully developed duct flow at $Re = 4600$, though these corner vortices were of lesser magnitude than those predicted by DNS at the same Reynolds number. The presence and strength of these corner vortices therefore represent convenient metrics for the zonally implemented QEVM.

The RANS simulations were performed with an in-house solver, SIERRA Fuego,[26] using the Launder and Sharma low-Reynolds number $k - \epsilon$ model.[27] SIERRA Fuego is a 3D control volume finite element method solver, and backward Euler time integration was employed as part of pseudo-transient time stepping to reach the steady state solution. First order upwind schemes were used for the convective terms of the momentum equations.

Since the flow is symmetric across the four corners of the duct, only one corner of the duct was modeled in the RANS simulations, and symmetry boundary conditions were imposed at the open faces. These RANS results will be compared to the DNS results of Pinelli et al.,[28] acquired at the same Reynolds number.

The zonal implementation of the quadratic eddy viscosity model was based on the machine learning classifier predictions of when the Reynolds stress anisotropy invariant II_b would be greater than 0.167. The resulting zonal mask of f_{ML} is shown in Fig. 2. As this figure shows, the anisotropy was predicted to be highest in the near-wall and corner regions of the flow, and so in the zonal QEVM simulation, the QEVM was applied in these regions of the flow.

2. Results

Because the duct flow is fully developed, it is sufficient to analyze a single streamwise plane of the simulation results. Figure 3 presents contours of streamwise velocity normalized by the centerline velocity U_{CL}, overlaid with secondary flow vectors. The DNS results show the presence of corner vortices in this flow that occupy the entire corner region. When using the LEVM, RANS is completely unable to predict any secondary flows, as indicated by the lack of any visible secondary flow vectors in Fig. 3(b). When the QEVM is implemented in Fig. 3(c), RANS successfully predicts the presence of corner vortices, of roughly the correct shape and location, though of reduced magnitude as compared to the DNS results. This result is consistent with that of Gnanga et al.,[25] who also reported that their non-linear eddy viscosity model produced corner vortices of reduced strength in comparison to their DNS results. When the QEVM is implemented zonally, as shown in Fig. 3(d), the corner vortices are weaker and confined to a narrow band near the wall.

In order to understand why the zonal implementation of the QEVM fails to predict the full extent of the corner vortices, it is useful to examine contours of II_b, as shown in Fig. 4(a). This figure shows that II_b only exceeds the threshold level for the machine learning classifier, 0.167, in a narrow band near the wall. The

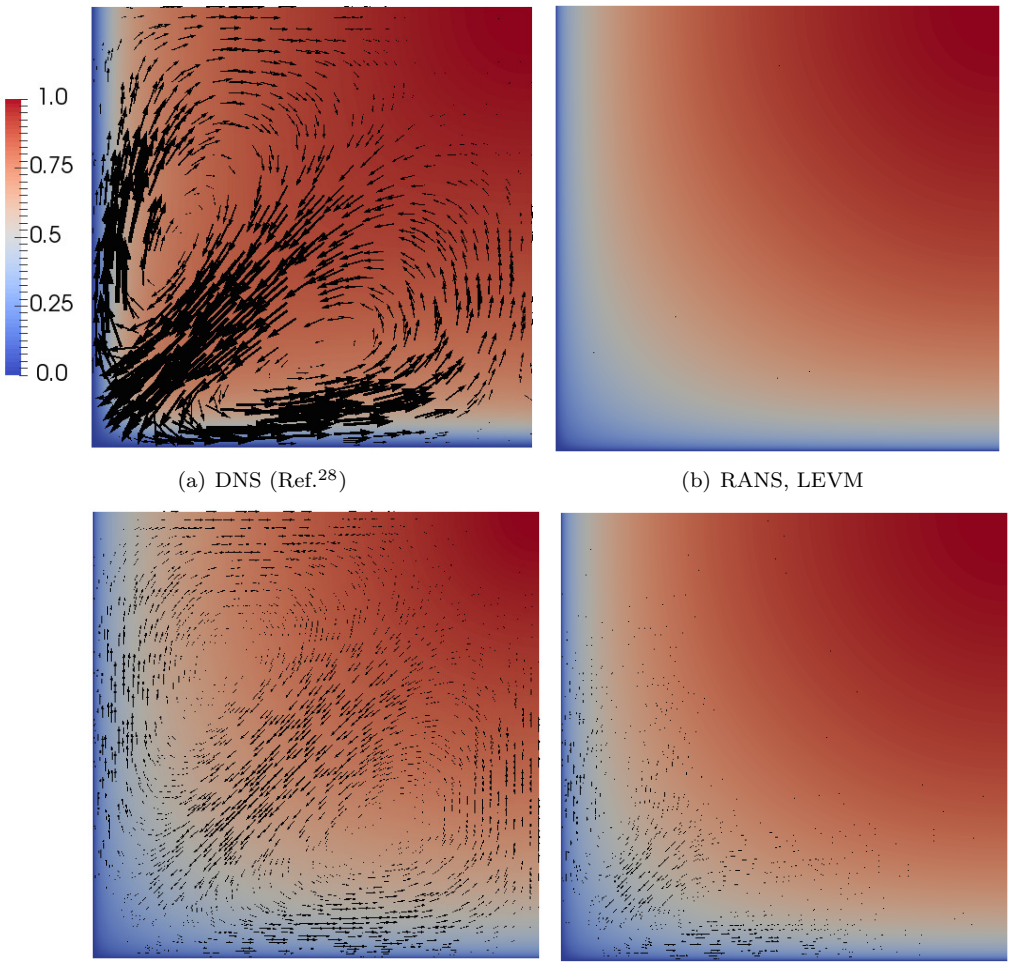

(a) DNS (Ref.[28])

(b) RANS, LEVM

(c) RANS, QEVM

(d) RANS, Zonal QEVM

Figure 3. Contours of streamwise velocity, normalized by centerline velocity. Secondary flow vectors overlaid in black.

zonal implementation based on this machine learning classifier therefore only implements the QEVM in this band. However, perhaps a lesser value of anisotropy is still enough to influence the flow. An alternate zonal mask, shown in Fig. 4(b), was formulated based on when II_b falls below 0.1. This zonal mask dictates that the QEVM be used for a much larger fraction of the duct cross-section. Figure 4(c) shows the RANS results when this mask is used to implement the zonal QEVM. As this figure shows, with this zonal implementation RANS predicts secondary flows very similar to those produced when employing QEVM globally.

These results therefore offer a caution to the zonal implementation: if the zones do not encompass the entire region over which the anisotropy is sufficient to affect the flow, then the resulting predictions will not be accurate. However, as demonstrated when using the second mask based on the lower threshold of II_b, once the entire region of significant Reynolds stress anisotropy is modeled using QEVM, the results closely match those produced by implementing QEVM globally.

B. Flow Over a Wavy Wall with Scalar Injection

1. Simulation Set-up

The second case study is of flow over a wavy wall with scalar injection, shown schematically in Fig. 5. A DNS for this flow configuration has been performed by Rossi,[29] and the flow set-up has been extensively documented in Ref.[29] The flow was periodic in the streamwise and spanwise directions, and the bottom wall

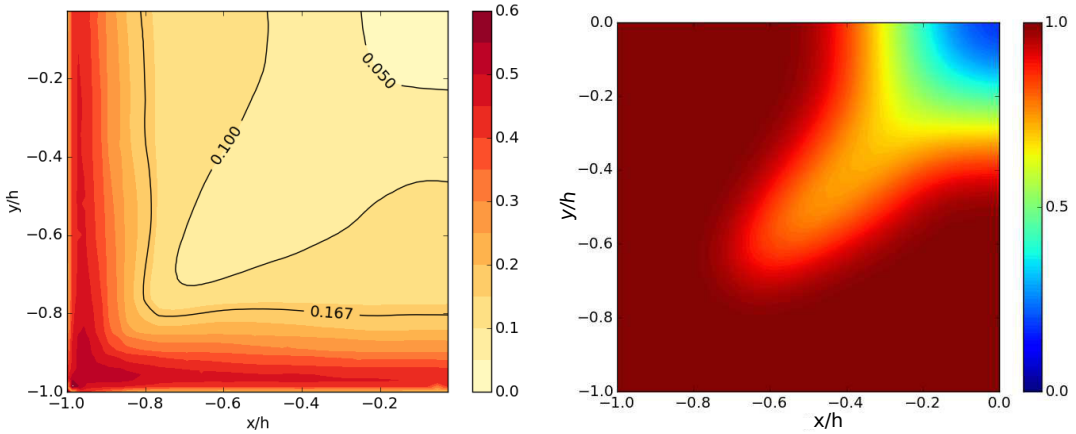

(a) Contours of II_b

(b) Zonal mask based on II_b

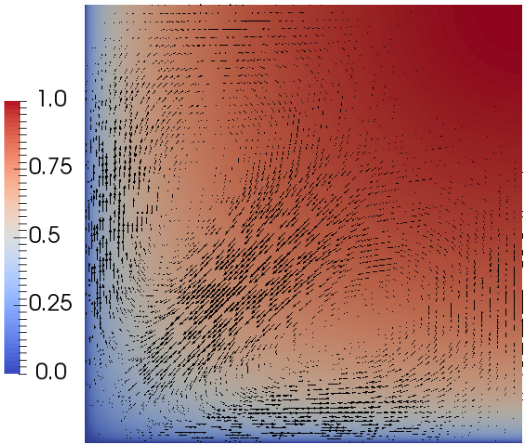

(c) Secondary flows for Zonal QEVM using mask based on II_b

Figure 4. (a) Contours of the second invariant of Reynolds stress anisotropy II_b, and (b) a zonal mask of f_{ML} based on when $II_b > 0.10$. Subfigure(c) shows contours of streamwise velocity, normalized by the centerline velocity, with secondary flow vectors overlaid in black, for a zonal implementation of QEVM using the mask specified in (b).

height y_w varied sinusoidally, with a wavelength λ equal to the mean channel height h and an amplitude of $0.05h$. The Reynolds number based on the mean inflow velocity and mean channel height was 7400. The passive scalar was injected from a point source at the top of a hill ($x/h = 1$), and the total mass flux from this injection point was 6 orders of magnitude less than the mass flux at the main inlet to the channel. This injection therefore had a negligible impact on the mean velocity field. The RANS boundary conditions were set to match those of the DNS of Rossi,[29] to allow direct comparison between these results.

The RANS simulations used the Launder-Sharma low Reynolds number $k - \epsilon$ model.[27] The baseline model used the LEVM with GDH to model the scalar transport. Previous studies by Rossi et al.[30,31] have shown that because GDH fails to accurately predict the flow anisotropy, particularly in the separated regions downstream of the hill crests, it under-estimates the lateral spread of the scalar. Rossi et al.[30,31] showed that the GGDH could more accurately predict this scalar dispersion. Therefore, the key question in this case study is whether or not a zonal implementation of QEVM with GGDH can predict the scalar dispersion as accurately as a global implementation of these RANS model corrections.

Figure 6 shows the machine learning-based mask of f_{ML} used for the zonal implementation of this model as prescribed by Eq. 5. As in the duct flow case, the Reynolds stress anisotropy tends to be high in the near wall regions, due to the no penetration condition at the walls. The anisotropy is particularly high on the leeward side of the hills.

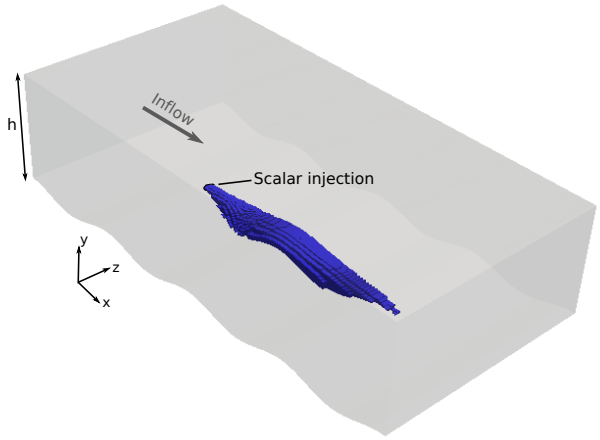

Figure 5. Schematic of flow configuration for flow over a wavy wall. An isosurface of scalar concentration, as predicted by RANS, is shown in blue.

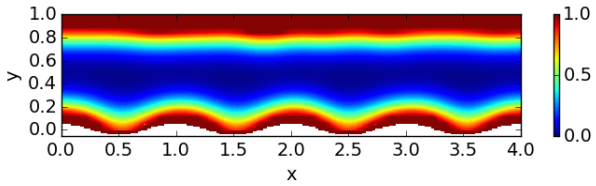

Figure 6. Mask of f_{ML} used for zonal implementation of QEVM and GGDH.

2. Results

Previous studies[30,31] have shown that RANS using the simple GDH model for turbulent scalar fluxes tends to under-estimate the dispersion of the passive scalar in this flow configuration. Figure 7 shows profiles of scalar concentration along the bottom wall at four streamwise locations. Results from the DNS of Rossi[29] are compared to RANS results using the LEVM with GDH, the QEVM with GGDH, and a zonal implementation of QEVM with GGDH.

As this figure shows, none of the RANS models are able to accurately replicate the DNS results at all locations. LEVM/GDH significantly over-predicts the scalar concentration near the mid-plane at $z = 0$. QEVM/GGDH is consistently more accurate than LEVM/GDH, particularly near injection. Furthermore, the results from the zonal implementation of QEVM/GGDH match those from the global implementation of QEVM/GGDH very closely. The only noticeable differences occur at the $x = 2$ streamwise location, but even at this location, the maximum discrepancy between the zonal and global implementation predictions of concentration was only 15%.

Figure 8 shows profiles of concentration in the y-direction at the channel mid-plane ($z = 0$) at specified streamwise locations. Once again, while neither QEVM/GGDH nor LEVM/GDH are able to successfully reproduce the DNS results, QEVM/GGDH is significant more accurate than LEVM/GDH at all profile locations. The blue shaded region on this figure indicates the region over which the QEVM/GGDH models are activated in the zonal implementation at each streamwise location. As this figure shows, the zonal QEVM/GGDH model provides a good match to the global QEVM/GGDH results even in the regions where the correction terms are not activated. These results demonstrate that implementing the RANS model corrections over a relatively small fraction of the flow designated by machine learning classifiers can successfully reproduce results obtained by a global implementation of these corrections.

One advantage of implementing the QEVM and GGDH models zonally instead of globally is that the zonal implementation significantly improved stability and convergence properties in this flow case. Many previous researchers[6,9–13] have remarked upon the degraded convergence and stability properties of anisotropic

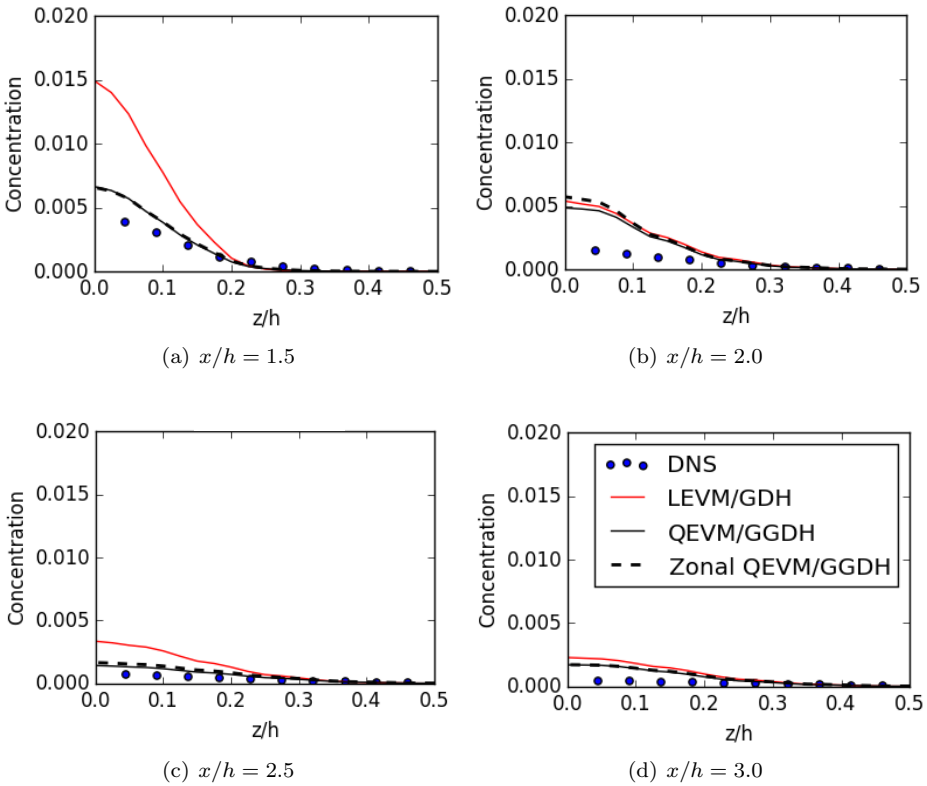

(a) $x/h = 1.5$ (b) $x/h = 2.0$

(c) $x/h = 2.5$ (d) $x/h = 3.0$

Figure 7. Profiles of scalar concentration along the bottom wall at four streamwise positions, as predicted by the DNS of Rossi[29] (circles), RANS LEVM/GDH (red line), RANS QEVM/GGDH (black line), and RANS with zonal QEVM/GGDH (dotted black line).

Reynolds stress and turbulent scalar flux models. In this case study, the zonal approach designates only a small fraction of the flow in which to apply the anisotropic models, resulting in improved convergence and stability relative to the global application of these models. Whereas the global implementation of these corrections required initializing the simulation from the converged LEVM/GDH solution in order to obtain convergence, the zonal implementation could be initialized from scratch with no problems. Furthermore, as pseudo-time-stepping was employed to march the solution toward steady state, larger time steps were possible when using the zonal implementation than when using the global implementation of QEVM with GGDH. For the zonal implementation, the CFL number could be set to 0.7, whereas this condition led to the growth of numerical instabilities for the global implementation. Figure 9 shows the concentration contours predicted by the zonal and global QEVM/GGDH models with CFL = 0.7; spurious oscillations are evident in the results from the global implementation. A lower value of CFL = 0.5 was required to reach convergence without these spurious oscillations with the global implementation. The relaxed requirements on both the initialization and time step suggest that the zonal implementation could provide faster solutions with better ease-of-use for the modeler.

Figure 10 shows the residuals for the continuity equation for three different simulations: LEVM/GDH, QEVM/GGDH, and zonal QEVM/GGDH. The residuals from the continuity equation are representative of the residuals from the other equations in the system in this case. For QEVM/GGDH, the simulation was initialized from the partially converged LEVM/GDH simulation in order to obtain convergence. As this plot shows, the zonal approach allows for faster convergence, both because it does not need to be initialized with an LEVM solution, and because it uses larger time steps. These results suggest that an adaptive physics modeling approach could provide improved stability and convergence in complex flow cases as compared to a global implementation of higher order RANS models. Furthermore, while the QEVM and GGDH models do not require significantly more computational power per iteration as compared to LEVM and GDH, many model corrections do require increased compute time. For example, Reynolds Stress Transport Models require

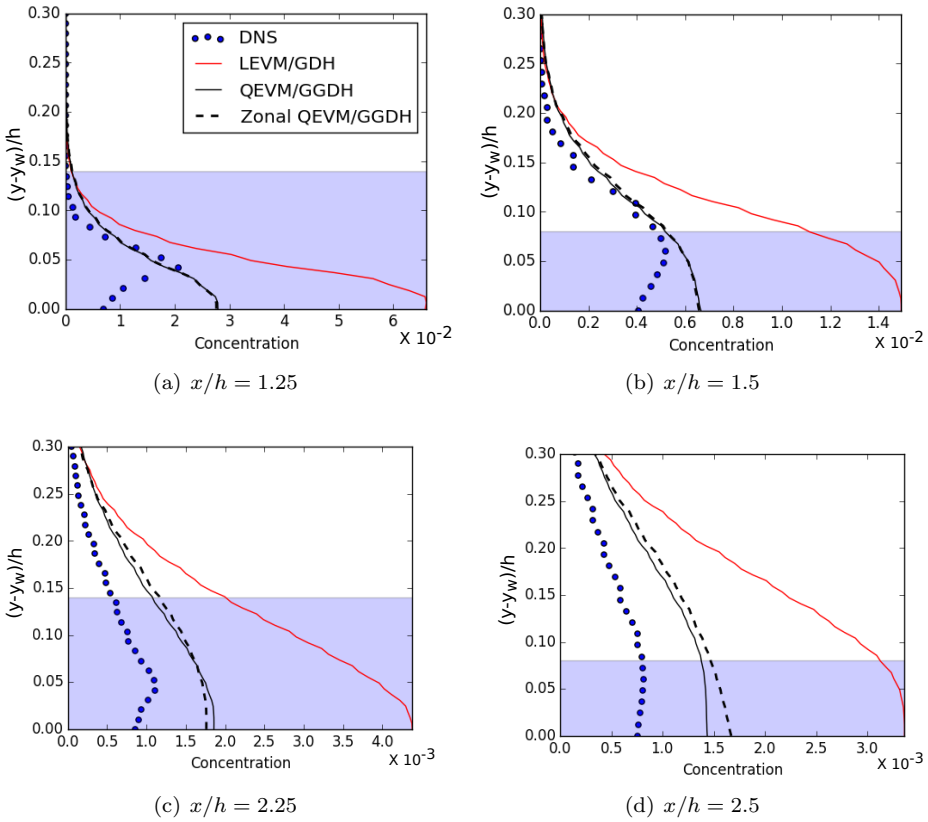

(a) $x/h = 1.25$ (b) $x/h = 1.5$

(c) $x/h = 2.25$ (d) $x/h = 2.5$

Figure 8. Vertical profiles of scalar concentration at four streamwise locations at the channel mid-plane ($z = 0$). Data from the DNS of Rossi[29] (circles), RANS LEVM/GDH (red line), RANS QEVM/GGDH (black line), and RANS with zonal QEVM/GGDH (dotted black line). The shaded blue region indicates the region over which the zonal correction is implemented in the zonal QEVM/GGDH case.

solving six extra transport equations for the Reynolds stresses. Zonal implementation of these models could provide not only increased stability, but also significant speed-up per step.

IV. Conclusions

A framework for data-driven adaptive physics modeling has been proposed. Machine learning classifiers, trained across a database of canonical flow configurations, can be used to flag regions of a flow in which underlying RANS model assumptions are violated. Higher order models or correction terms can be implemented zonally in these regions, mitigating the source of model form uncertainty.

The key question investigated was whether a zonal implementation of RANS model corrections in regions flagged by machine learning classifiers could provide the same accuracy as a global implementation of the same corrections. The adaptive physics modeling framework was evaluated for two test cases: fully developed duct flow and flow over a wavy wall with scalar injection. In the case of fully developed duct flow, it was shown that a zonal implementation of a quadratic eddy viscosity model was as effective as a global implementation at predicting the stress-driven secondary flows only when the zonal implementation occurred over the entire region with non-negligible Reynolds stress anisotropy. Implementing the QEVM over a smaller region with the highest levels of Reynolds stress anisotropy led to reduced strength and extent in the predicted secondary flow structures.

For the wavy wall flow configuration, a zonal implementation of the anisotropic eddy viscosity and turbulent scalar flux models successfully reproduced the improved scalar dispersion predictions of the global implementation of these models. Furthermore, in this flow configuration, the zonal implementation demonstrated improved stability and convergence properties relative to the global implementation of the anisotropic

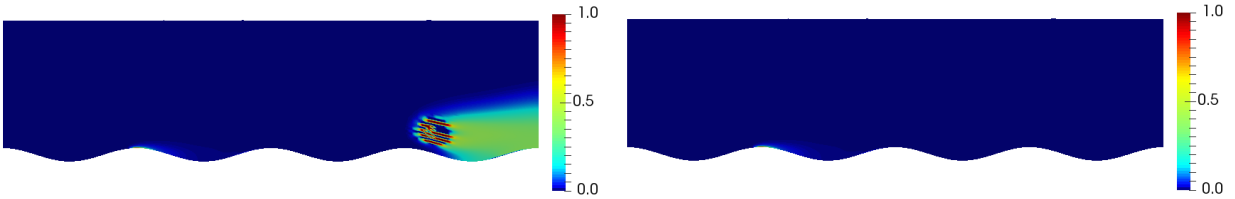

(a) Global QEVM/GGDH (b) Zonal QEVM/GGDH

Figure 9. Contours of scalar concentration at the channel mid-plane ($z = 0$) as predicted by the (a) global and (b) zonal implementations of QEVM/GGDH at a solver CFL number of 0.7. This CFL number leads to numerical instabilities in the global implementation but not in the zonal implementation.

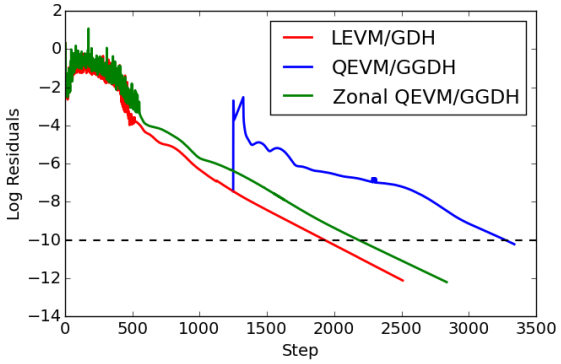

Figure 10. Normalized log residuals for the continuity equation versus simulation step number for RANS LEVM/GDH (red), RANS QEVM/GGDH (blue), and RANS zonal QEVM/GGDH (green). The dashed line indicates when residuals have decayed by 10 orders of magnitude.

models, suggesting that zonal implementation of RANS correction terms could provide an optimal combination of improved predictive accuracy without the implementation challenges often associated with these higher order models.

It should be noted that in both of the flow cases investigated in this study, while the anisotropic RANS models provided improved accuracy over the default isotropic RANS models, they did not provide a perfect match to the DNS data. The adaptive physics modeling framework proposed in this paper is general in its scope, and could be used to trigger higher fidelity turbulence models such as Reynolds Stress Transport Models or Large Eddy Simulations in the regions of high model form uncertainty, instead of simple RANS corrections such as QEVM and GGDH. Machine learning methods could also be used to provide more accurate closure models. This paper demonstrates that if the RANS model is corrected in the regions of the flow in which the RANS assumptions break down, then the RANS model form error is mitigated to the same extent that a global application of the correction terms would have achieved. Data-driven machine learning methods provide the critical information of which regions require the higher order model form. This zonal implementation achieves a compromise of improved accuracy with minimal impact to convergence and stability.

Acknowledgments

The authors wish to thank V. Brunini for his valuable support in the code implementation stage of this research, S. Bova and G. Lacaze for their helpful feedback on the manuscript, and R. Rossi for his generosity in sharing his data. Funding for this work was provided by the Sandia LDRD program, and its support is gratefully acknowledged. Sandia National Laboratories is a multi-program laboratory managed and operated by Sandia Corporation, a wholly owned subsidiary of Lockheed Martin Corporation, for the U.S. Department

of Energy's National Nuclear Security Administration under contract DE-AC04-94AL85000.

References

[1]H.N. Najm. Uncertainty quantification and polynomial chaos techniques in computational fluid dynamics. *Annual Review of Fluid Mechanics*, 41:35–52, 2009.

[2]T.A. Oliver and R.D. Moser. Bayesian uncertainty quantification applied to RANS turbulence models. *Journal of Physics: Conference Series*, 318:042032, 2011.

[3]J. Ray, S. Lefantzi, S. Arunajatesan, and L. Dechant. Bayesian calibration of a $k-\epsilon$ turbulence model for predictive jet-in-crossflow simulations. *AIAA 44th Fluid Dynamics Conference*, 2014.

[4]C.Gorle, J. Larsson, M. Emory, and G. Iaccarino. The deviation from parallel shear flow as an indicator of linear eddy-viscosity model inaccuracy. *Physics of Fluids*, 26:051702, 2014.

[5]S. Wallin and A.V. Johansson. An explicit algebraic Reynolds stress model for incompressible and compressible turbulent flows. *Journal of Fluid Mechanics*, 403:89–132, 2000.

[6]T.B. Gatski and C.G. Speziale. On explicit algebraic stress models for complex turbulent flows. *Journal of Fluid Mechanics*, 254:59–78, 1993.

[7]W. Rodi. A new algebraic relation for calculating the Reynolds stresses. *Gesellschaft Angewandte Mathematik und Mechanik Workshop Paris France*, 56:219, 1976.

[8]T.J. Craft, B.E. Launder, and K. Suga. Development and application of a cubic eddy-viscosity model of turbulence. *International Journal of Heat and Fluid Flow*, 17:108–115, 1996.

[9]L. Belhoucine, M. Deville, A.R. Elazehari, and M.O. Bensalah. Explicit algebraic Reynolds stress model of incompressible turbulent flow in a rotating square duct. *Computers and Fluids*, 33:179–199, 2004.

[10]M.M. Rahman, P. Rautaheimo, and T. Siikonen. Modifications for an explicit algebraic stress model. *International Journal for Numerical Methods in Fluids*, 35:221–245, 2001.

[11]G.J. Easom N.G. Wright. Non-linear k-ϵ turbulence model results for flow over a building at full-scale. *Applied Mathematical Modeling*, 27:1013–1033, 2003.

[12]W.L. Chen, F.S. Lien, and M.A. Leschziner. Computational prediction of flow around highly loaded compressor cascade blades with non-linear eddy-viscosity models. *International Journal of Heat and Fluid Flow*, 19:307–319, 1998.

[13]T.J. Craft, H. Iacovides, and J.H. Yoon. Progress in the use of non-linear two-equation models in the computation of convective heat-transfer in impinging and separated flows. *Flow, Turbulence and Combustion*, 63:59–80, 1999.

[14]J. Ling and J.A. Templeton. Evaluation of machine learning algorithms for prediction of regions of high RANS uncertainty. *Physics of Fluids*, 27:085103, 2015.

[15]M. Berger and J. Oliger. Adaptive mesh refinement for hyperbolic partial differential equations. *Journal of Computational Physics*, 53:484–512, 1984.

[16]M.J. Berger and P. Colella. Local adaptive mesh refinement for shock hydrodynamics. *Journal of Computational Physics*, 82:64–84, 1989.

[17]Z.J. Zhang and K. Duraisamy. Machine learning methods for data-driven turbulence modeling. *AIAA Aviation*, pages 2015–2460, 2015.

[18]J. Ling, A. Kurzawski, and J. Templeton. Reynolds averaged turbulence modelling using deep neural networks with embedded invariance. *Journal of Fluid Mechanics*, 807:155–166, 2016.

[19]S.B. Pope. A more general effective-viscosity hypothesis. *Journal of Fluid Mechanics*, 72:331–340, 1975.

[20]W.P. Jones and B.E. Launder. The prediction of laminarization with a two-equation model of turbulence. *International journal of heat and mass transfer*, 15:301–314, 1972.

[21]B. Daly and F. Harlow. Transport equations in turbulence. *Physics of Fluids*, 13:2634–2649, 1970.

[22]S.B. Pope. *Turbulent Flows*. Cambridge University Press, 2000.

[23]D.R. Radenkovic, J.M. Burazer, and D.M. Novkovic. Anisotropy analysis of turbulent swirl flow. *FME Transactions*, 42:19–25, 2014.

[24]P. Bradshaw. Turbulent secondary flows. *Annual review of fluid mechanics*, 19:53–74, 1987.

[25]H. Gnanga, H. Naji, and G. Mompean. Computation of a three-dimensional turbulent flow in a square duct using a cubic eddy-viscosity model. *Comptes Rendus Mecanique*, 337:15–23, 2009.

[26]S.P. Domino, C.D. Moen, S.P. Burns, and G.H. Evans. SIERRA/Fuego: A multi-mechanics fire environment simulation tool. *AIAA Aerospace Sciences Meeting*, 2003.

[27]B.E. Launder and B.I. Sharma. Application of the energy-dissipation model of turbulence to the calculation of flow near a spinning disc. *Letters in heat and mass transfer*, 1:131–137, 1974.

[28]A. Pinelli, M. Uhlmann, A. Sekimoto, and G. Kawahara. Reynolds number dependence of mean flow structure in square duct turbulence. *Journal of Fluid Mechanics*, 644:107–122, 2010.

[29]R. Rossi. Passive scalar transport in turbulent flows over a wavy wall. Doctoral thesis, Universita degli Studi di Bologna, Bologna, Italy, 2006.

[30]R. Rossi. A numerical study of algebraic flux models for heat and mass transport simulation in complex flows. *International Journal of Heat and Mass Transfer*, 53:4511–4525, 2010.

[31]R. Rossi, D. Philips, and G. Iaccarino. A numerical study of scalar dispersion downstream of a wall-mounted cube using direct simulations and algebraic flux models. *International Journal of Heat and Fluid Flow*, 31:805–819, May 2010.